

## First results of baryon interactions from lattice QCD with physical masses (2) — S=-3 and S=-4 sectors ( $\Xi\Xi$ , $\Xi\Sigma$ , $\Xi\Lambda$ - $\Xi\Sigma$ channels)—

---

Noriyoshi Ishii<sup>\*,ab</sup>, Sinya Aoki,<sup>bcd</sup> Takumi Doi,<sup>b</sup> Shinya Gongyo,<sup>bc</sup> Tetsuo Hatsuda,<sup>be</sup>  
Yoichi Ikeda,<sup>b</sup> Takashi Inoue,<sup>bf</sup> Takumi Iritani,<sup>bg</sup> Takaya Miyamoto,<sup>bc</sup> Keiko  
Murano,<sup>ab</sup> Hidekatsu Nemura,<sup>bd</sup> Kenji Sasaki<sup>bd</sup>

<sup>a</sup> Research Center for Nuclear Physics (RCNP), Osaka University, Osaka 567-0047, Japan

<sup>b</sup> Theoretical Research Division, Nishina Center, RIKEN, Wako 351-0198, Japan

<sup>c</sup> Yukawa Institute for Theoretical Physics, Kyoto University, Kyoto 606-8502, Japan

<sup>d</sup> Center for Computational Sciences, University of Tsukuba, Ibaraki 305-8571, Japan

<sup>e</sup> Kavli IPMU (WPI), The University of Tokyo, Chiba 277-8583, Japan

<sup>f</sup> Nihon University, College of Bioresource Sciences, Kanagawa 252-0880, Japan

<sup>g</sup> Department of Physics and Astronomy, Stony Brook University, Stony Brook, New York  
11794-3800, USA

E-mail: ishiin@rcnp.osaka-u.ac.jp

We present our preliminary lattice QCD results of baryon-baryon potentials in  $S = -3$  and  $S = -4$  sectors from almost the physical point by using the 2+1 flavor gauge configurations generated on  $96^4$  lattice with  $a \simeq 0.085$  fm and  $L = 96a \simeq 8.2$  fm where  $m_\pi \simeq 146$  MeV and  $m_K \simeq 525$  MeV.

*The 33rd International Symposium on Lattice Field Theory  
14 -18 July 2015  
Kobe International Conference Center, Kobe, Japan\**

---

\*Speaker.

## 1. Introduction

Experimental determination of hyperon potentials is one of the most important projects in nuclear physics. In J-PARC experiment, they are mainly interested in determining the hyperon potentials in  $S = -1$  and  $S = -2$  sectors. Experimental determination of hyperon potentials become more difficult for increasing number of strange quarks because of the short life time of the strange quark. In contrast, lattice QCD calculation becomes easier for increasing number of strange quarks, because the statistical noise reduces. In this paper, we use HAL QCD method [1, 2, 3] to construct the hyperon potentials in  $S = -3$  and  $S = -4$  sectors based on the Nambu-Bethe-Salpeter (NBS) wave functions generated by lattice QCD. We give our preliminary results by using the 2+1 flavor gauge configurations at almost the physical point generated by using K computer at AICS.

## 2. Lattice QCD setup

We use the 2+1 flavor gauge configurations at almost the physical point generated by K computer at AICS. It is generated on  $96^4$  lattice by employing the RG improved (Iwasaki) gauge action at  $\beta = 1.82$  together with the nonperturbatively  $O(a)$ -improved Wilson quark (clover) action at  $(\kappa_{\text{ld}}, \kappa_{\text{s}}) = (0.126117, 0.124790)$  with  $c_{\text{SW}} = 1.11$  and the 6-APE stout smeared links with the smearing parameter  $\rho = 0.1$ . It corresponds to the lattice cutoff  $a^{-1} \simeq 2.3$  GeV ( $a \simeq 0.085$  fm), the spatial extension  $L = 96a \simeq 8.2$  fm,  $m_\pi \simeq 146$  MeV, and  $m_K \simeq 525$  MeV [4, 5]. 200 gauge configurations are used. Measurements are performed with the wall source at 12 source points. Quark propagators are obtained by imposing the periodic boundary condition along the spatial direction, while Dirichlet boundary condition is imposed on the temporal direction on the time slice  $t = t_1$  which is separated from the wall source as  $t_1 - t_0 = 48$ . Forward and backward propagations are combined by using the charge conjugation and time-reversal symmetry to double the statistical data of two-point and four-point hyperon correlators. Each gauge configuration is used 4 times by using the hypercubic  $SO(4, \mathbb{Z})$  symmetry of the  $96^4$  lattice. Statistical data are averaged in the bin of the size 10. Jackknife prescription is used to estimate the statistical errors.

## 3. $S = -4$ sector ( $\Xi\Xi$ channel)

To construct the  $\Xi\Xi$  potentials, we define R-correlator for  $\Xi\Xi$  as

$$R_{\Xi\Xi}(\vec{x} - \vec{y}, t) \equiv e^{2m_\Xi t} \langle 0 | T [\Xi(\vec{x}, t) \Xi(\vec{y}, t) \bar{\mathcal{J}}_{\Xi\Xi}(t=0)] | 0 \rangle, \quad (3.1)$$

where  $m_\Xi$  denotes the mass of  $\Xi$ ,  $\Xi(\vec{x}, t)$  the local composite interpolating field for  $\Xi$ , and  $\bar{\mathcal{J}}_{\Xi\Xi}$  the wall source for  $\Xi\Xi$ . The exponential factor  $e^{2m_\Xi t}$  is used to subtract the rest mass of two  $\Xi$ 's. In Ref[6], the R-correlator Eq. (3.1) is shown to satisfy the time-dependent Schrödinger-like equation

$$\left( \frac{1}{4m_\Xi} \frac{\partial^2}{\partial t^2} - \frac{\partial}{\partial t} + \frac{\nabla^2}{m_\Xi} \right) R_{\Xi\Xi}(\vec{r}, t) = \int d^3 r' V_{\Xi\Xi}(\vec{r}, \vec{r}') R_{\Xi\Xi}(\vec{r}', t), \quad (3.2)$$

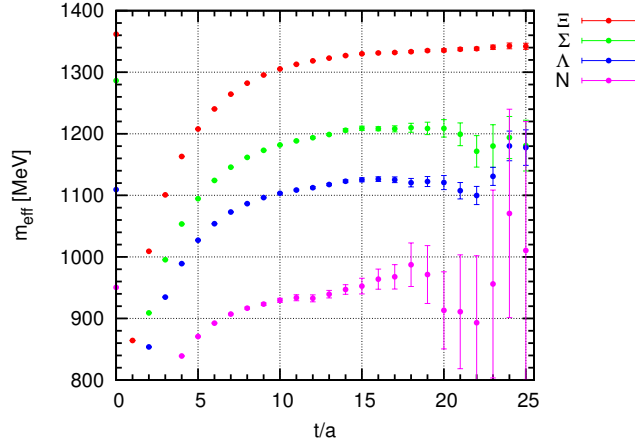
by using the spectral decomposition of Eq. (3.1), the Schrödinger equation satisfied by the energy-independent HAL QCD potential, and the identity which involves the ‘‘relative momentum’’  $k$  and

the relativistic total energy  $E$  in the C.M. frame as

$$\frac{k^2}{m_{\Xi}} = \frac{1}{4m_{\Xi}} (E - 2m_{\Xi})^2 + (E - 2m_{\Xi}) \quad \text{with} \quad E \equiv 2\sqrt{m_{\Xi}^2 + k^2}, \quad (3.3)$$

The time-dependent Schrödinger-like equation Eq. (3.2) enables us to extract the HAL QCD potential without requiring the ground state saturation of  $R_{\Xi\Xi}(t)$ . All which is required is to achieve the elastic saturation so that the intermediate states should be dominated by the contributions below the inelastic threshold. Note that the elastic saturation is much easier to be achieved than the ground state saturation especially when the spatial volume is large.

In a practical calculation, we replace the factor  $e^{2m_{\Xi}t}$  in  $R_{\Xi\Xi}(\vec{r}, t)$  by  $C_{\Xi}(t)^{-2}$  where  $C_{\Xi}(t)$  denotes the two point temporal correlator of the local composite  $\Xi$  field with wall source so that the correlated statistical noises may cancel. For this replacement, the single state saturation of  $C_{\Xi}(t)$  is required. The effective mass plot of  $C_{\Xi}(t)$  is shown in Fig. 1.



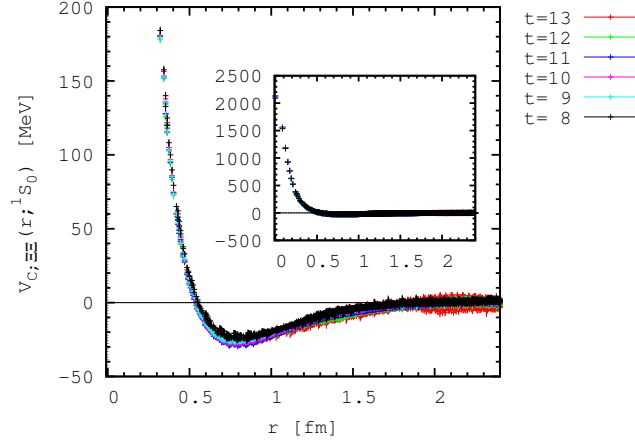
**Figure 1:** The effective mass plot of baryonic two point correlators with wall source.

Fig. 2 shows the result of the central potential of  $\Xi\Xi$  in  $^1S_0$  with  $I = 1$  obtained from  $t = 8 - 13$ . We see that it has a repulsive core at short distance which is surrounded by an attraction. Qualitative behavior is similar to the NN potential in  $^1S_0$  channel. This is because both of  $\Xi\Xi$  ( $I = 1$ ) and NN ( $I = 1$ ) belong to the same flavor irreducible representation (irrep.) **27** in the flavor SU(3) limit.

Fig. 3 shows the results of the central potential (left) and the tensor potential (right) of  $\Xi\Xi$  in  $^3S - D_1$  with  $I = 0$  obtained from  $t = 8 - 13$ . We see that the central potential has a repulsive core at short distance. There may be an attraction at the medium distance. To confirm its existence, statistics has to be increased. The tensor potential is weak and positive <sup>1</sup>.  $\Xi\Xi$  with  $I = 0$  belongs to the flavor irrep. **10** in the flavor SU(3) limit. As a result, their qualitative behaviors are similar to the baryon-baryon potentials for the irrep. **10** given in Ref.[8]. Note that  $N\Sigma$  ( $I = 3/2$ ) belongs to the irrep. **10**, but NN does not belong to it.

In these calculations, we show the results which are obtained from the time slice  $t = 8 - 13$ . In the effective mass plot Fig. 1, the two point temporal correlator of  $\Xi$  with wall source shows the

<sup>1</sup>The tensor potential is obtained by using the method given in Ref.[7].



**Figure 2:** The central potential  $V_C$  for  $\Xi\Xi$  in  $^1S_0$  ( $I = 1$ ).

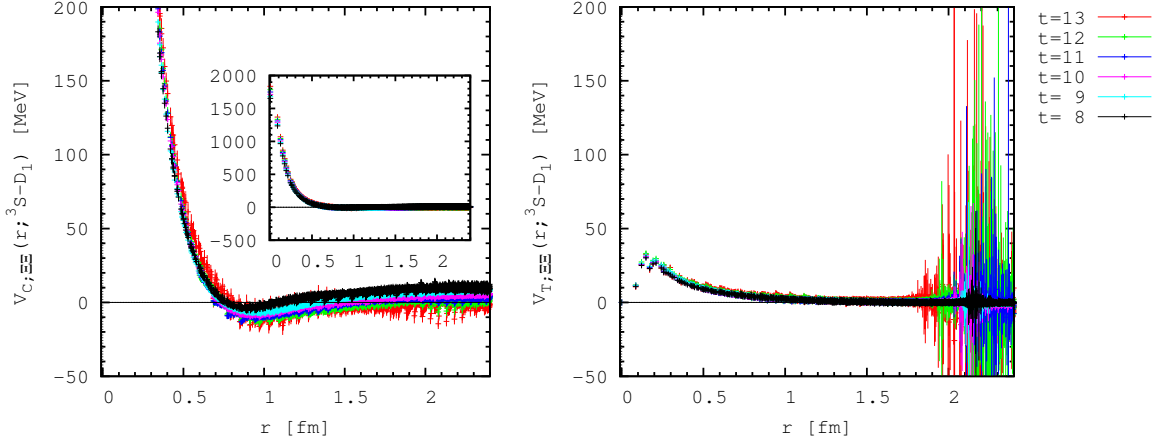


**Figure 3:** The central potential  $V_C$  (left) and the tensor potential  $V_T$  (right) for  $\Xi\Xi$  for  $^3S-D_1$  ( $I = 0$ ).

plateau in the region  $t \gtrsim 15$ . Although the  $t$ -dependence of the results of the potentials is seen to be mild, the results can have sizable contamination from excited states. It is desirable to go to the larger  $t$  region, for which statistics has to be increased.

#### 4. $S = -3$ sector ( $\Xi\Sigma(I = 3/2)$ channel)

$\Xi\Sigma$  potentials for  $I = 3/2$  are constructed from the R-correlator for  $\Xi\Sigma$  defined as

$$R_{\Xi\Sigma}(\vec{x} - \vec{y}, t) \equiv e^{(m_\Xi + m_\Sigma)t} \langle 0 | T [\Xi(\vec{x}, t) \Sigma(\vec{y}, t) \mathcal{J}_{\Xi\Sigma}(t=0)] | 0 \rangle, \quad (4.1)$$

where  $m_\Sigma$ ,  $\Sigma(\vec{y}, t)$  denote the mass of  $\Sigma$  and the local composite interpolating field for  $\Sigma$ , respectively.  $\mathcal{J}_{\Xi\Sigma}$  denotes the wall source for  $\Xi\Sigma$  ( $I = 3/2$ ). Since  $m_\Xi \neq m_\Sigma$ ,  $R_{\Xi\Sigma}$  satisfies a different time-dependent Schrödinger-like equation from Eq. (3.2). Instead of using Eq. (3.3), we use [9]

$$k^2 E^2 = \frac{1}{4} (E^2 - (m_\Xi + m_\Sigma)^2) (E^2 - (m_\Xi - m_\Sigma)^2) \quad \text{with} \quad E \equiv \sqrt{m_\Xi^2 + k^2} + \sqrt{m_\Sigma^2 + k^2}. \quad (4.2)$$

A similar argument leads us to another time-dependent Schrödinger-like equation

$$D_{\Xi\Sigma} R_{\Xi\Sigma}(\vec{r}, t) = \int d^3 r' V_{\Xi\Sigma}(\vec{r}, \vec{r}') D_{t; \Xi\Sigma}^2 R_{\Xi\Sigma}(\vec{r}', t), \quad (4.3)$$

with

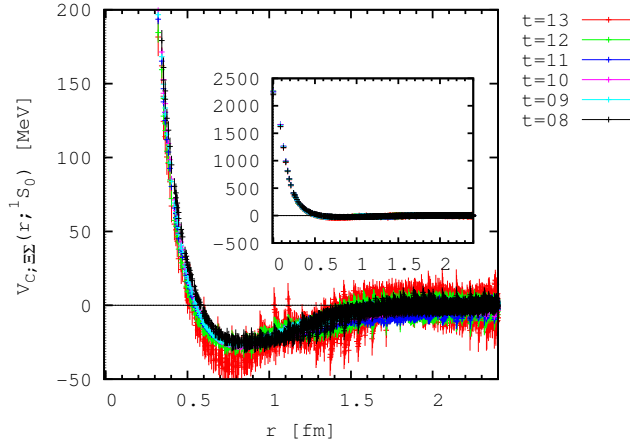
$$D_{\Xi\Sigma} \equiv \frac{\nabla^2}{2\mu_{\Xi\Sigma}} D_{t; \Xi\Sigma}^2 + \frac{1}{8\mu_{\Xi\Sigma}} (D_{t; \Xi\Sigma}^2 - (m_{\Xi} + m_{\Sigma})^2) (D_{t; \Xi\Sigma}^2 - (m_{\Xi} - m_{\Sigma})^2), \quad (4.4)$$

where  $D_{t; \Xi\Sigma} \equiv \partial_t - m_{\Xi} - m_{\Sigma}$  and  $\mu_{\Xi\Sigma} \equiv \frac{1}{1/m_{\Xi} + 1/m_{\Sigma}}$  denotes the reduced mass. Note that Eq. (4.3) involves the fourth time derivative, for which the numerical differentiation is still unstable. In this paper, we use a non-relativistically approximated equation

$$\left( \frac{\nabla^2}{2\mu_{\Xi\Sigma}} - \frac{\partial}{\partial t} \right) R_{\Xi\Sigma}(\vec{r}, t) = \int d^3 r' V_{\Xi\Sigma}(\vec{r}, \vec{r}') R_{\Xi\Sigma}(\vec{r}', t). \quad (4.5)$$

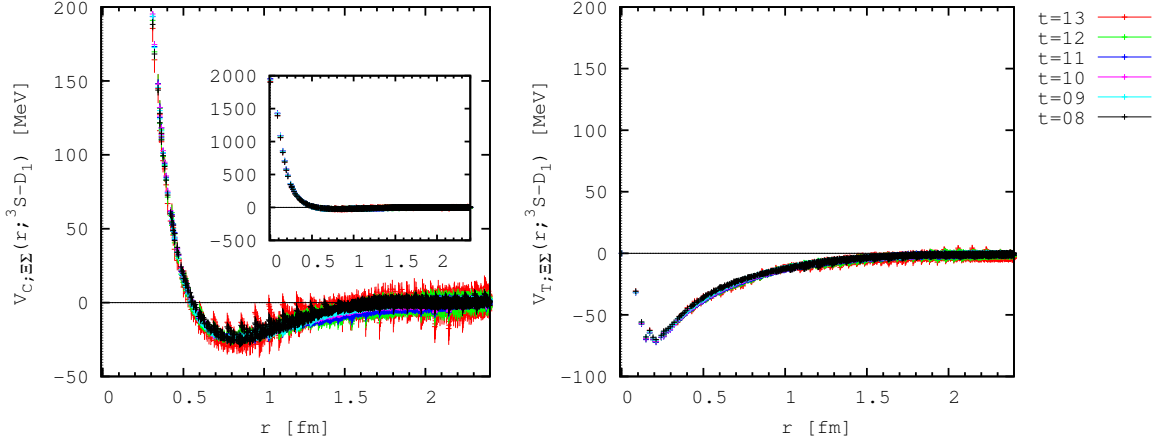
We expect the approximation Eq. (4.5) to work, because the intermediate states of  $R_{\Xi\Sigma}(\vec{r}, t)$  which is constructed with the wall source are dominated by low-energy contributions. Due to the similar reason as  $\Xi\Xi$  potentials, we replace the factors  $e^{m_{\Xi}t}$  and  $e^{m_{\Sigma}t}$  by  $C_{\Xi}(t)^{-1}$  and  $C_{\Sigma}(t)^{-1}$ , respectively, in practical calculations, where  $C_{\Sigma}(t)$  denotes the two point temporal correlator of the local composite  $\Sigma$  field with wall source. The ground state saturations of these two-point correlators are required for Eq. (4.5) to work. The effective mass plot of these correlators is given in Fig. 1.

Fig. 4 shows the central potential for  $\Xi\Sigma$  ( $I = 3/2$ ) in  $^1S_0$  obtained from  $t = 8 - 13$ . We see that it has a repulsive core at short distance, which is surrounded by an attraction. In this way, qualitative behavior is similar to the NN potential. This is natural, because both  $\Xi\Sigma$  ( $I = 3/2$ ) and NN ( $I = 1$ ) belong to the same flavor irrep.  $\mathbf{27}$  in the flavor SU(3) limit.



**Figure 4:** The central potential for the single channel  $\Xi\Sigma$  ( $I = 3/2$ ) in  $^1S_0$ .

Fig. 5 shows the central potential (left) and the tensor potential (right) for  $\Xi\Sigma$  ( $I = 3/2$ ) in  $^3S_1 - D_1$  obtained from  $t = 8 - 13$ . We see that their qualitative behaviors are quite similar to the NN potentials, i.e., the central potential has a repulsive core at short distance which is surrounded by an attraction, and the tensor potential has a quite similar shape as NN tensor potential. Since both  $\Xi\Sigma$  ( $I = 3/2$ ) and NN ( $I = 0$ ) belong to the same irrep.  $\mathbf{10}^*$ , the similarity is natural.



**Figure 5:** The central and the tensor potentials for the single channel  $\Xi\Sigma$  ( $I = 3/2$ ) in  ${}^3S - D_1$ .

These potentials are obtained from the time slice  $t = 8 - 13$ . However, Fig. 1, the effective mass plot of the two point temporal correlators of  $\Xi$  and  $\Sigma$  show the plateau in the regions  $t \gtrsim 15$ . Although the  $t$ -dependence of these potentials are small, it is desirable to go to the larger  $t$  region in the future by increasing the statistics.

### 5. $S = -3$ sector ( $\Xi\Lambda$ - $\Xi\Sigma$ ( $I = 1/2$ ) channel)

To obtain the  $\Xi\Lambda$ - $\Xi\Sigma$  potentials, we consider the two R-correlators as

$$\begin{aligned} R_{\Xi\Lambda}(\vec{x} - \vec{y}, t; \mathcal{J}) &\equiv e^{(m_{\Xi} + m_{\Lambda})t} \langle 0 | T [\Xi(\vec{x}, t) \Lambda(\vec{y}, t) \mathcal{J}(t=0)] | 0 \rangle \\ R_{\Xi\Sigma}(\vec{x} - \vec{y}, t; \mathcal{J}) &\equiv e^{(m_{\Xi} + m_{\Sigma})t} \langle 0 | T [\Xi(\vec{x}, t) \Sigma(\vec{y}, t) \mathcal{J}(t=0)] | 0 \rangle, \end{aligned} \quad (5.1)$$

where  $m_{\Lambda}$  and  $\Lambda(\vec{y}, t)$  denote the mass of  $\Lambda$  and the local composite  $\Lambda$  field, respectively.  $\mathcal{J} \equiv \mathcal{J}_{\Xi\Lambda}, \mathcal{J}_{\Xi\Sigma}$  denote wall sources for  $\Xi\Lambda$  and  $\Xi\Sigma$  ( $I = 1/2$ ), respectively. By using a similar arguments, these R-correlators are found to satisfy a coupled channel generalization of the time-dependent Schrödinger-like equation

$$\begin{pmatrix} D_{\Xi\Lambda} R_{\Xi\Lambda}(\vec{r}, t; \mathcal{J}) \\ D_{\Xi\Sigma} R_{\Xi\Sigma}(\vec{r}, t; \mathcal{J}) \end{pmatrix} = \int d^3 r' \begin{pmatrix} V_{\Xi\Lambda; \Xi\Lambda}(\vec{r}, \vec{r}') & \zeta^{+t} V_{\Xi\Lambda; \Xi\Sigma}(\vec{r}, \vec{r}') \\ \zeta^{-t} V_{\Xi\Sigma; \Xi\Lambda}(\vec{r}, \vec{r}') & V_{\Xi\Sigma; \Xi\Sigma}(\vec{r}, \vec{r}') \end{pmatrix} \begin{pmatrix} D_{t; \Xi\Lambda}^2 R_{\Xi\Lambda}(\vec{r}, t; \mathcal{J}) \\ D_{t; \Xi\Sigma}^2 R_{\Xi\Sigma}(\vec{r}, t; \mathcal{J}) \end{pmatrix}. \quad (5.2)$$

Here  $\zeta \equiv e^{(m_{\Sigma} - m_{\Lambda})}$ , and  $D_{\Xi\Lambda}$  denotes the differential operator defined as

$$D_{\Xi\Lambda} \equiv \frac{\nabla^2}{2\mu_{\Xi\Lambda}} D_{t; \Xi\Lambda}^2 + \frac{1}{8\mu_{\Xi\Lambda}} (D_{t; \Xi\Lambda}^2 - (m_{\Xi} + m_{\Lambda})^2) (D_{t; \Xi\Lambda}^2 - (m_{\Xi} - m_{\Lambda})^2), \quad (5.3)$$

where  $\mu_{\Xi\Lambda} \equiv \frac{1}{1/m_{\Xi} + 1/m_{\Lambda}}$  denotes the reduced mass of  $\Xi$  and  $\Lambda$ , and  $D_{t; \Xi\Lambda} \equiv \partial_t - m_{\Xi} - m_{\Lambda}$ . Note that there are four central potentials ( $\Xi\Lambda$ - $\Xi\Sigma$  coupled channel) in  ${}^1S_0$ , and four central and four tensor potentials ( $\Xi\Lambda$ - $\Xi\Sigma$  coupled channel) in  ${}^3S - D_1$ . Numerical results are coming. We will present them somewhere else.

## 6. Summary

We have presented our preliminary results of central and tensor hyperon potentials of  $\Xi\Xi$  and  $\Xi\Sigma(I = 3/2)$  by using the 2+1 flavor gauge configurations at almost the physical point ( $m_\pi \sim 146$  MeV) on the huge spatial volume  $L \sim 8.2$  fm generated by K computer at AICS. We have used the time-dependent HAL QCD method to obtain these potentials. We have seen that, as far as these potentials are concerned, the qualitative behaviors are similar to those in flavor SU(3) limit. These potentials have been obtained from  $t = 8 - 13$ , where the potentials show mild  $t$ -dependence. Although their  $t$ -dependences are mild, these  $t$  regions are smaller than the plateau regions of temporal two-point correlators of  $\Xi$  and  $\Sigma$ . It is desirable to go to the larger  $t$  region in the future by increasing the statistics. Indeed, we plan to improve the statistics by 8 times soon.

Due to the limited time, we have not shown the results of coupled channel potentials for  $\Xi\Lambda$ - $\Xi\Sigma(I = 1/2)$ , which we will present somewhere else in the near future.

## Acknowledgments

Lattice QCD calculations have been performed on the K computer at RIKEN, AICS (Nos. hp120281, hp130023, hp140209, hp150223), HOKUSAI FX100 computer at RIKEN, Wako (No.G15023) and HA-PACS at University of Tsukuba (Nos. 14a-20, 15a-30). We thank ILDG/JLDG [10] which serves as an essential infrastructure in this study. This work is supported in part by MEXT Grant-in-Aid for Scientific Research (15K17667, 25287046, 25400244, 26400281) and SPIRE (Strategic Program for Innovative REsearch) Field 5 project. We thank all collaborators in this project.

## References

- [1] N. Ishii, S. Aoki and T. Hatsuda, Phys. Rev. Lett. **99** (2007) 022001 doi:10.1103/PhysRevLett.99.022001 [nucl-th/0611096].
- [2] S. Aoki, T. Hatsuda and N. Ishii, Prog. Theor. Phys. **123** (2010) 89 doi:10.1143/PTP.123.89 [arXiv:0909.5585 [hep-lat]].
- [3] S. Aoki *et al.* [HAL QCD Collaboration], PTEP **2012** (2012) 01A105 doi:10.1093/ptep/pts010 [arXiv:1206.5088 [hep-lat]].
- [4] Y. Taniguchi, PoS LATTICE **2012** (2012) 236 [arXiv:1303.0104 [hep-lat]].
- [5] K.-I. Ishikawa *et al.*, PoS LATTICE **2015** (2015) 075 [arXiv:1511.09222 [hep-lat]].
- [6] N. Ishii *et al.* [HAL QCD Collaboration], Phys. Lett. B **712** (2012) 437 doi:10.1016/j.physletb.2012.04.076 [arXiv:1203.3642 [hep-lat]].
- [7] K. Murano *et al.* [HAL QCD Collaboration], Phys. Lett. B **735** (2014) 19 doi:10.1016/j.physletb.2014.05.061 [arXiv:1305.2293 [hep-lat]].
- [8] T. Inoue *et al.* [HAL QCD Collaboration], Nucl. Phys. A **881** (2012) 28 doi:10.1016/j.nuclphysa.2012.02.008 [arXiv:1112.5926 [hep-lat]].
- [9] T. Doi, private communication.
- [10] <http://www.lqcd.org/ildg/> and <http://www.jldg.org/>